J. Condensed Matter Nucl. Sci. 40 (2025) 48–58

Research Article

Stimulation of Efficient Low Energy Tritium Fusion Under The Action of a Weak Undamped Thermal Wave on Remote TiD Target

Vladimir I. Vysotskii
Taras Shevchenko National University of Kyiv, Ukraine

Alla A. Kornilova
Member of Condensed Matter Nuclear Science Society, AVSystems Inc., 54, Harpsichord TPKE, Stamford, USA

Sergey N. Gaydamaka
AVSystems Inc., 54, Harpsichord TPKE, Stamford, USA

Abstract

This study investigates the implementation of (dd) low-energy nuclear reactions (LENR) under the influence of an undamped weak thermal (temperature) wave on a remote *TiD* target. These waves are generated in the air during the cavitation of a water jet in a closed chamber. The research reveals that the rate of tritium fusion is approximately 10^8 times greater than the rate of helium fusion in these (dd) reactions.

Keywords: Undamped thermal waves, Coherent correlated states, Low energy nuclear reactions

1. Introduction

It is widely acknowledged that current methods and projects aimed at achieving nuclear fusion are fraught with significant technological challenges. This paper explores a potential mechanism for stimulating LENR involving the generation, propagation, and distant influence of thermal waves. Contrary to the conventional understanding that such waves rapidly dampen, transforming into an unstructured thermal field, our investigation challenges this notion. The classical thermodynamic perspective assumes that the non-equilibrium system under study can be represented as numerous small local equilibrium subsystems. The mathematical description of this process relies on the simultaneous application of two fundamental equations:
the Fourier law for nonstationary heat flux $\vec{q}(\vec{r},t)$

$$\vec{q}(\vec{r},t) = -\lambda \cdot grad(T(\vec{r},t)) \tag{1}$$

and the equation of continuity

$$\rho c_v \frac{\partial T(\vec{r},t)}{\partial t} = div\vec{q}(\vec{r},t). \tag{2}$$

Here λ, ρ and c_v are coefficients of heat transfer, density, and specific heat.

From (1) and (2) follows the usual wave equation for the temperature field and thermal waves

$$\rho c_v \frac{\partial T(\vec{r},t)}{\partial t} = div\left\{\lambda grad[T(\vec{r},t)]\right\}. \tag{3}$$

The solutions of this equation in 1D case are two colliding plane thermal (temperature) waves

$$T(\omega,x,t) = A_\omega e^{-\kappa x} e^{i(\omega t-\kappa x)} + B_\omega e^{\kappa x} e^{i(\omega t+\kappa x)} \tag{4}$$

with a significant damping coefficient equal to the wave number κ:

$$\delta \equiv \kappa = \sqrt{\omega/2G}. \tag{5}$$

Here $G = \lambda/\rho c_v$ is a coefficient of thermal diffusivity.

Notably, the conventional "standard" thermal wave (4) demonstrates attenuation over a spatial distance equivalent to the wavelength, and we have $\delta \approx 10^4\ cm^{-1}$ and attenuation length of $\delta^{-1} \approx 1\ \mu\mathrm{m}$ for air at $\omega = 80\ MHz$. However, it becomes apparent that the standard classical equations of thermodynamics (1–3) were derived under inaccurate assumptions, failing to consider relaxation processes. The solution (4) for thermal waves is valid solely for low-frequency heat waves.

2. Fundamental Concepts of Undamped Thermal Waves Theory

Equations (1–3) are founded on the approximate assumption that the energy thermal flow $\vec{q}(\vec{r},t)$ and temperature $T(\vec{r},t)$ change synchronously within any small area along the wave propagation trajectory. This traditional yet erroneous assumption is rectified through a detailed analysis, revealing that a formal decrease in microvolume does not correspond to a decrease in relaxation time. The latter necessitates a substantial number (approximately $\sim$10) of collisions between atoms and molecules. For accurate analysis, the continuity equation (1) must be modified with a time shift τ and considering the portion of the equation influenced by thermal action - whether it involves the change in temperature $T(\vec{r},t)$ over time within the microvolume due to introduced energy

$$div\vec{q}(\vec{r},t) \Rightarrow -\rho c_v \frac{\partial T(\vec{r},t+\tau)}{\partial t}, \tag{6}$$

or the change in the flow $\vec{q}(\vec{r},t)$ in space resulting from temperature changes

$$\rho c_v \frac{\partial T(\vec{r},t-\tau)}{\partial t} \Rightarrow -div\vec{q}(\vec{r},t). \tag{7}$$

The time shifts in both equations, determined by identical relaxation processes, can be assumed with high accuracy to be identical and equal to the thermodynamic relaxation time τ. As heat waves propagate, these processes remain interconnected, compelling the consideration of both equation variants. Consequently, a joint analysis of these equations, along with Fourier's law (1) for nonstationary heat flow $\vec{q}(\vec{r},t)$, yields a modified equation of thermal conductivity that incorporates the time delay (relaxation time τ) [1]–[5]:

$$\frac{\partial T(\vec{r},t\pm\tau)}{\partial t} = G\nabla^2 T(\vec{r},t) \tag{8}$$

The solution of the corrected equation (8) in 1D case can be presented as a superposition of colliding waves:

$$\begin{aligned} T(\omega,x,t) &= A_\omega \mathrm{e}^{-\delta x}\mathrm{e}^{i(\omega t-k'x)} + B_\omega \mathrm{e}^{\delta \mathrm{x}}\mathrm{e}^{i(\omega t+kx)} \\ &\equiv A_\omega \exp\left(-\kappa\left|\cos\frac{\omega\tau}{2}\pm\sin\frac{\omega\tau}{2}\right|x\right)\exp\left\{i\left(\omega t-\kappa\left|\cos\frac{\omega\tau}{2}\mp\sin\frac{\omega\tau}{2}\right|x\right)\right\} \\ &\quad +B_\omega \exp\left(\kappa\left|\cos\frac{\omega\tau}{2}\pm\sin\frac{\omega\tau}{2}\right|x\right)\exp\left\{i\left(\omega t+\kappa\left|\cos\frac{\omega\tau}{2}\mp\sin\frac{\omega\tau}{2}\right|x\right)\right\}. \end{aligned} \quad (9)$$

These waves correspond to the wave number and absorption coefficient

$$k=\kappa|\cos(\omega\tau/2)\pm\sin(\omega\tau/2)|, \quad (10)$$

$$\delta=\kappa|\cos(\omega\tau/2)\mp\sin(\omega\tau/2)|,\ \kappa=\sqrt{\omega/2G}. \quad (11)$$

Temperature waves with characteristic frequencies

$$\omega_n=(2n+1)\pi/2\tau, \quad n=0,1,2,\ldots \quad (12)$$

are undamped temperature waves ($\delta=0$) and they have wave number $\kappa_{\text{eff}}=\kappa(\omega_n)\sqrt{2}$:

$$T(\omega_n,x,t)=A_{\omega_n}\exp\left\{i\left(\omega_n t-\kappa\sqrt{2}x\right)\right\}+B_{\omega_n}\exp\left\{i\left(\omega_n t+\kappa\sqrt{2}x\right)\right\}. \quad (13)$$

The frequencies of these waves, under typical air parameters, are determined by

$$\omega_n\approx 80\cdot(2n+1)\ MHz, \quad n=0,1,2,\ldots \quad (14)$$

These waves, characterized by their ability to propagate over long distances without attenuation, act effectively on distant targets. Their short wavelength results in a minimal diffraction expansion of their flow. Undamped waves are not only generated during precisely periodic heating with frequencies ω_n (12) applied to a layer of air or a surface bordering air but also during pulsed short-term heating with a duration Δt shorter than the relaxation time τ in air (during such pulses the spectrum of generated thermal waves will contain spectral components with a frequency ω_n (12)).

In our experiments, a pulsed method was employed, utilizing short shock waves generated during cavitation of a water jet emerging from a narrow channel into the closed volume of the cavitation chamber (Fig. 1). These experiments used ordinary drinking water (not distilled). In this system, cavitation was formed when a water jet exited through a steel channel with a diameter of about 2 *mm* into the closed chamber. The working pressure of water in this system corresponded to 150 *atmospheres*. The cavitation target was made from a steel plate approximately 2.5 *mm* thick.Thermal waves were generated by excitation or ionization and subsequent rapid decay or recombination of atoms on the outer surface of a flat cavitation target under the influence of acoustic shock waves formed by the interaction of water with cavitation bubbles with the inner surface of the target. Soft X-ray radiation with an energy of approximately $\hbar\omega_X \approx 1.5\ keV$, produced during decay or recombination, was absorbed rapidly in the air, heating it and leading to the excitation of thermal waves. The emitted X-ray radiation was effectively detected by an X-spectrometer or photographic plates near the outer surface [3]–[5].

Thermal waves were generated by excitation or ionization and subsequent rapid decay or recombination of atoms on the outer surface of a flat cavitation target under the influence of acoustic shock waves formed by the interaction of water with cavitation bubbles with the inner surface of the target.

The study of these undamped thermal waves involved their interaction, entailing rapid heating and cooling, with the surface of a piezocrystal in a remote acoustic detector. The resultant rapid temperature changes induced acoustic waves in the piezocrystal, recorded by the detector. These waves, recorded [4], [5] at distances of up to 2 *m* at frequencies corresponding to ω_n (12), with a maximum frequency reaching 1 *GHz*. The registration range was constrained by the size of the laboratory.

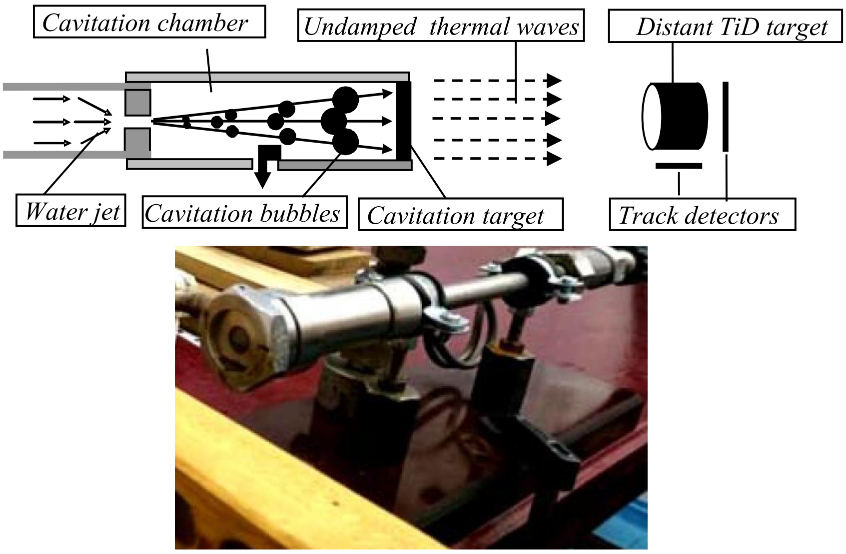

Figure 1. Scheme of experiments on the generation of undamped temperature waves and stimulation of nuclear fusion in a distant target and general view of the experimental setup.

It is necessary to take into account the structural features of the thermal wave at a relatively short distance from its source. Such a wave is a set of harmonics within the spectral interval $|\omega - \omega_n| \leq \Delta\omega$, close to optimal frequencies ω_n. These harmonics exhibited weak attenuation in air, forming a pulsed wave packet of short duration $\Delta t \approx 1/\Delta\omega$. Our calculations [1]–[5] and conducted experiments demonstrate that the action of these waves on a distant nuclear active target leads to the effective stimulation of nuclear reactions.

3. Stimulation of D-D Reactions in Distant Targets by Undamped Thermal Waves

3.1. Prerequisites of stimulating fusion by heat wave

One of the possible application of undamped thermal ways [5]–[7] is connected with direct distant stimulation of nuclear dd-fusion

$$\begin{aligned} &d + d = He^3(0,82\ MeV) + n(2,45\ MeV), \\ &d + d = H^3(1,01\ MeV) + p(3,02\ MeV), \\ &d + d = He^4(76\ keV) + \gamma(23.1\ MeV) \end{aligned} \tag{15}$$

The mutual redistribution of the energy of each of these reactions between the products of these reactions at low energies of their collisions corresponds to the laws of conservation of energy and momentum. Very short-term energy fluctuations associated with the uncertainty relation allow the Coulomb barrier to be overcome, but do not affect the final energy distribution among the products of these reactions.

The first two reactions correspond to the direct reaction, and in the third reaction a compound nucleus is formed. In standard thermonuclear fusion physics using really (not virtually) accelerated particles, the probabilities of the first two channels of fusion are approximately equal and the probability of the third channel of fusion (15) is very small.

For the initial deuterons, with low average real (not virtual) energy, the probability of the first reaction, with a proton being captured by a moving H^2 nucleus, is very small compared to the second reaction, due to the Oppenheimer-Phillips effect (the mutual reorientation of two interacting H^2 nuclei, resulting in the capture of a neutron and the formation of a nucleus H^3 and a free proton). At the same time, it should be recalled that the total probability of both of these reactions at low real energy will be very small due to the low probability of the tunnel effect.

For particles with high real energy, the duration of both direct reactions (in fact, the duration of the mutual counter-flight) is very small, which leads to the impossibility of mutual reorientation of these nuclei and to the same probability of the capture of a proton or neutron by a moving deuteron.

For the case of direct reactions with low average energy in the presence of a short time $\delta\mathrm{t}$ and large energy fluctuation δE, the third (alternative) option should be realized - a high probability of reaction and the fulfillment of the condition of selective neutron capture with the formation of He^3 nucleus.

For the third reaction (15) at a low average temperature of the material environment, a very low energy of the formed alpha particle is characteristic. The mean free path in air of alpha particles from the third reaction with such energy 76 keV does not exceed 0.01 *cm* and cannot be registered by a distant (5 *mm*) track detector.

For this reason, the most likely reactions observed in these experiments involve the formation of He^3 and H^3 particles. Stimulation of these reactions occurs through several successive stages. Initially, rapid temperature changes on the surface of the target result in the generation of shock waves within the target volume. These shock waves, in turn, influence the state of deuterium localized in the nanocracks of the *TiD* target or in the spaces between *Ti* atoms in the *TiD* lattice. The modulation of parameters of these potential wells at the nanoscale, as revealed by direct analysis [10]–[17], leads to the formation of a coherent correlated state (CCS) of deuterons. The potential existence of such quantum states was initially contemplated by Schrödinger and Robertson [18], [19]. The creation of CCS is intricately tied to the optimal phase synchronization of quantum states of a particle in a superposition state within a nonstationary potential well.

When a deuteron is localized within a typical interatomic interval $a \approx 2\,\mathring{A}$ or within a nanocrack of size $a \approx 10 - 20\,\mathring{A}$, the energy fluctuation in CCS surpasses the value

$$\delta E \geq G^2\hbar^2(2N+1)/8M(\delta\mathrm{x})^2 \geq 10 - 30\ keV. \quad (16)$$

Here, $\delta x \approx a/2$, $G \equiv 1/\sqrt{1-r^2} \approx 10^3 - 10^4$ is the realistic coefficient of correlation efficiency, and $N = 0, 1, 2, \ldots$ is the number of the energy level of the deuteron in this potential well before the impact of the shock wave. At room temperature of the target $N \approx 5 - 50$ for interatomic potential wells or nanocracks in titanium, respectively.

The substantial increase in particle energy fluctuation δE during CCS formation is linked to the Schrödinger-Robertson uncertainty relation [18], [19] and is associated with the further development of this method applied to nuclear physics problems [11]–[17].

It is very important that in CCS formed during modulation of a potential well, both the amplitude δE of kinetic energy fluctuations and the duration δt of these fluctuations increase very significantly compared to the "usual" Heisenberg uncertainty relation $\delta t \geq \hbar/\delta E$. It was shown [16], [17] that without such increase of δt, no nuclear reactions would be possible.

Our experiments [20] have unveiled a significant impact of thermal waves on the structure of distant crystalline targets. In this study, we have examine the phase composition and structure of one titanium (*Ti*) sample and two *Ti* samples saturated with deuterium (*D*) at 150%, both before and after irradiation with thermal waves. The investigation was conducted using an X-ray diffractometer with a rotating copper anode. Notably, a five-minute irradiation of two identical $TiD_{1.5}$ samples and one pure *Ti* sample with thermal waves at a distance of 20 *cm* resulted in a substantial compression of their crystal lattices, as detailed in Table 1.

Table 1. Deformation (compression) of a crystalline target after irradiation by a thermal wave

Test sample	Crystal lattice period, $\AA$ (before irradiation)	Crystal lattice period, $\AA$ (after irradiation for 5 minutes)
Ti	2.939 and 4.691	2.927 and 4.669
$TiD_{1.5}$(1)	4.404	4.396
$TiD_{1.5}$(2)	4.403	4.399

It is evident that local and instantaneous (with subsequent return) deformations of the crystal lattice at the locations of nanocracks and impurity deuterium nuclei could exceed these values. These findings affirm the significant influence of the irradiation process on the dynamic microstructure of the irradiated targets.

3.2. Stimulation of He^3 Fusion in a Remote *TiD* Target

Experiments were conducted to implement the $d + d = He^3 + p$ channel of the (dd)-reaction (15), leading to the formation of He^3 nuclei. The experimental setup, as illustrated in Fig. 1, utilized a *TiD* target (length – *L* = 10 *mm*, diameter – *D* = 7 *mm*, saturation $\sim$150%) and track detectors. The titanium sample was saturated using a standard method in a special closed chamber at a high pressure of about 1 atm of gaseous deuterium and a temperature of 300–350^{0}C. Repeat studies using an X-ray diffractometer after 0.5 year, 1 year and 3 years showed that the original high density of deuterium in the target remained unchanged.

The *TiD* target was positioned approximately 20 *cm* away from the cavitation chamber.

For He^3 track analysis, a plastic CR-39 type detector made of polycarbonate (polyallyl diglycol) with a density of 1.3 *g/cm*^{3} and a thickness of 1 *mm* ("TASTRAK^{tm}" detector from Track Analysis Systems Ltd, Bristol, UK) was employed. Standard experimental conditions involved placing the detector 5 *mm* away from the surface of the target, subject to the thermal wave for specific durations (20 and 40 *minutes*). Post-irradiation, the detector underwent 6.25-M etching using a *NaOH* solution for 3.5 *hours* at a temperature of $80°C$.

The image of tracks was photographed using an Olympus BX-51 optical microscope with the Image Scope M program.

In Fig. 2a, a photograph of a track detector is presented, positioned 5 *mm* behind the reverse end surface (relative to the thermal wave source) of the cylindrical TiD target.

Fig. 2b shows a photograph of a fragment of a similar flat track detector located parallel to the side surface of the same cylindrical TiD target at a distance of 5 *mm*.

Both detectors were exposed for the same time (40 *minutes*). In Fig. 2a and 2b, the directions of movement of heavy charged particles (nuclei 3) when they hit the surface of the track detector are indicated by arrows. There were no traces of tracks on the back of the track detector.

For control purposes, Fig. 2c presents a segment of a comparable track detector irradiated with a reference "triplet" alpha radiation mixed source: U^{233}, Pu^{238}, and Pu^{239}. The energies of alpha particles He^4 emitted during the decay of these isotopes are respectively equal to 4.679 *MeV*, 5.593 *MeV* and 5.157 *MeV* [21].

Another proof of the reliability of the implemented nuclear fusion of He^3 nuclei is the axial symmetry of the tracks on Fig. 2b, which corresponds to the cylindrical shape of the *TiD* target and the spatial symmetry of the thermal waves that irradiate this target. In the hypothetical presence of background alpha-like radiation (for example, in the presence of radon gas), the orientation of these tracks would be completely random. In addition, similar track detectors stored in the same laboratory, in the absence of such irradiation by a thermal wave, remain without any tracks on both its surfaces even during long-term storage.

A detailed analysis of the experiment on the fusion of He^3 nuclei in a remote target under the influence of a thermal wave is presented in Table 2.

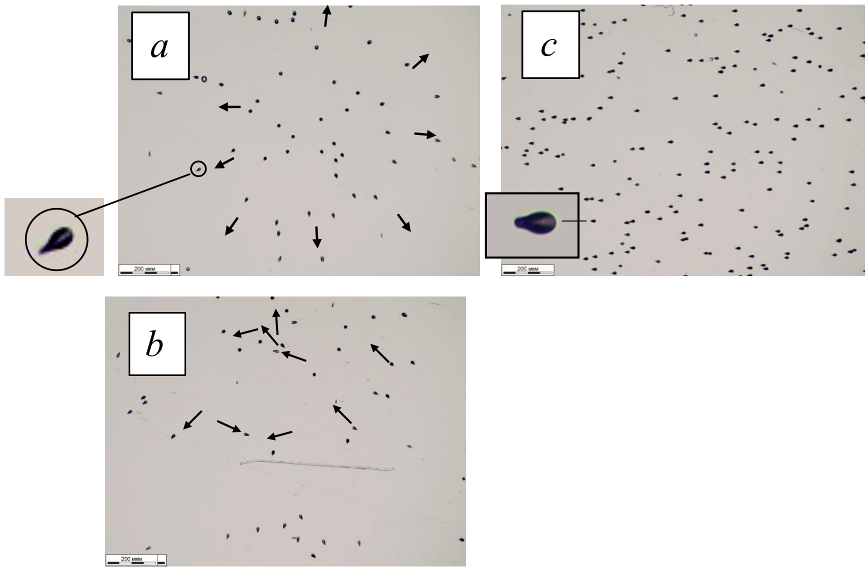

Figure 2. a) Track analysis showing the movement of heavy charged particles produced in a distant *TiD* target the opposite end surface of which was irradiated with thermal radiation for 40 minutes. b) Photograph of a fragment of a similar flat track detector located parallel to the side surface of the same cylindrical TiD target. c) Photograph of a similar track detector irradiated with a reference alpha emitter based on a three radionuclides: U^{233}, Pu^{238}, Pu^{239}. The directions of movement of nuclei 3 when they hit the surface of the track detector are indicated by arrows.

Table 2. Measured and estimated parameters of alpha particle fusion stimulated thermal wave

Thermal wave irradiation of the *TiD* target	Number of registered alpha-tracks	Full flux of alpha particles on the reverse surface *S* of the target	The total number of $d(d,p)He^3$ reactions in target volume upon irradiation with a thermal wave	The rate of stimulated nuclear alpha particle fusion during thermal wave irradiation of the target
T_0 = 40 minutes	N_0 = 52	$N_s \approx$ 1000 (taking into account absorption in air and in near-surface layer of *TiD* target)	$N_0 \approx \frac{2N_s L}{<l_{He^3}>} \approx 2{\cdot}10^7$ (estimation)	$\eta_{H^3} = \frac{N_0}{\mathrm{LS} n_{H^2} T_0} \approx 2.2 \cdot 10^{-19}$*created* He^3 *nuclei/s*$\cdot H^2$ *nucleus*

Here $<l_{He^3}> \approx 1.25$ μm is He^3 nucleus free path in *Ti*; $n_{H^2} = 1.5 \cdot n_{\mathrm{Ti}} \approx 8.2 \cdot 10^{22} cm^{-3}$ is the concentrations of *D* atoms in *TiD* target; *S* = 0.38 cm^2 is the surface of the target's back end.

3.3. Stimulation of Tritium Fusion in a Remote *TiD* Target

An evaluation of the efficiency of the alternative (dd)-reaction $d + d \to H^3 + p$ was conducted on the same samples after a period of t_0 = 6 *months* following irradiation with a temperature wave for 20 or 40 *minutes*. This delay in measurement was chosen to ensure the presence of long-lived synthesized H^3 nuclei. This analysis utilized a radioluminescence method, accounting for the spatial position and beta activity of the resulting H^3 nuclei with a half-life $T_{1/2} = \tau_T ln2 = 12.3$ *years* in irradiated *TiD* targets.

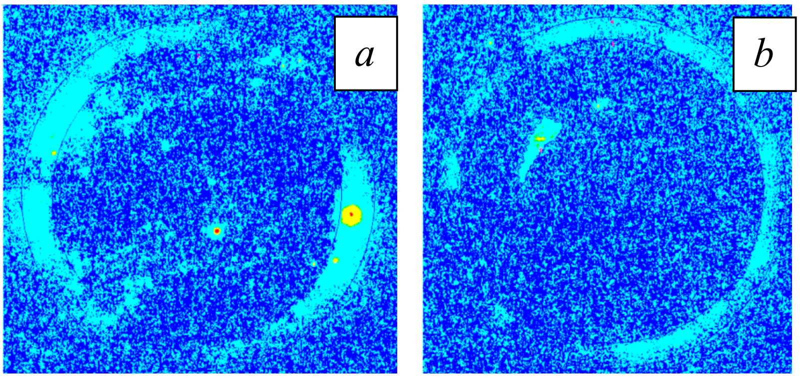

Figure 3. Photographs of radioluminograms formed upon irradiation of radioluminogram plate with electrons created during the beta decay of tritium, which was synthesized by the action of a temperature wave on distant *TiD* targets for 40 *minutes* (a) and 20 *minutes* (b).

Table 3. β^- activity of *TiD* targets irradiated 6 monthes ago by the thermal waves

Thermal wave irradiation time	Duration of rendering by *HeNe* laser beam	Surface of active radioluminogram,	Total surface directonal β^- activity Q_s, *Bk* (toward detector)
T_0 = 40 *min*	65 *hours*	1.05 cm^2	163.5
T_0 = 20 *min*	65 *hours*	0.88 cm^2	40.5

Fig. 3 presents photographs of two radioluminograms illustrating the spatial distribution and concentration of synthesized tritium in the *TiD* target area near the rear (end) surface.

Fig. 3a corresponds to the target irradiated for 40 *minutes*, and Fig. 3b corresponds to 20 *minutes*.

The absence of radioactive background in the laboratory is also confirmed by the result that the concentration of registered active centers on the back side of the *TiD* targets increases approximately proportionally to the duration of irradiation with a thermal wave (20 and 40 *min*).

These radioluminograms result from *HeNe* laser imaging (photostimulated luminescence) of latent images formed in irradiated phosphor plates by β^- during $H^3 = He^3 + \beta^- + \widetilde{\nu}$ decay. The radioluminogram plate consists of a 50 μm thick luminescent layer and a 410 μm thick substrate. The luminescent layer comprises a mixture of phosphor $BaFBrEu^{2+}$ and crystal-binding phosphor polymer (*C*/*H*/*N*/*O* = 8/12/2/1) in a composition ratio of 20:1 by weight. The substrate consists of a layer of polyethylene terephthalate with a thickness of 250 μm, covering the base of ferrite 160 μm thick. Specific radiation dose determination is achieved by comparison with a special standard Amershan reference plate containing 16 known levels of tritium activity. Upon exposure to beta particles emitted by tritium, electronic *F* centers and hole centers ($Eu^{2+} \rightarrow Eu^{3+}$) are formed. This system of centers creates a latent distribution image of tritium on the imaging plate.

After contact with the radioactive sample under study, the plate is placed in the reader, where, under the action of a focused laser beam, photostimulated luminescence occurs sequentially at each point. Under the influence of *HeNe* laser radiation in the red range ($\lambda \approx$ 633 *nm*), electrons are released from F-centers and annihilate with Eu^{3+} hole centers, forming Eu^{2+} ions in the excited state, which, in less than one millisecond, return to the ground state. During this process, radiation quanta are emitted with a wavelength belonging to the blue-violet range of the visible spectrum ($\lambda \approx$ 390 *nm*). These quanta enter a photomultiplier through a light guide and are recorded as an analog electrical signal, subsequently converted into a digital signal.

The β^- activity parameters recorded from these radioluminograms are presented in Table 3.

Table 4. Parameters of tritium fusion in *TiD* target irradiated with a thermal wave

Thermal wave irradiation time	Total volume beta activity (estimated value), *Bk/TiD* target	Total concentration of created tritium nuclei (estimated value), cm^{-3}	The rate of total tritium fusion by thermal wave in $d+d=H^3+p$ reaction, $cm^{-3}\ s^{-1}$
$T_0 = 40\ min$	$Q_{\text{total}} \approx \frac{2Q_S L}{<l_b>} \approx 10^7$	$n_{\text{total}} = \frac{Q_{\text{total}}\ \tau_T}{\text{L S}e^{-T_0/\tau_T}} \approx 4 \cdot 10^{15}$	$\alpha = \frac{n_{\text{total}}}{T_0} \approx 1.7 \cdot 10^{12} cm^{-3} s^{-1}$
$T_0 = 20\ min$	$Q_{\text{total}} \approx 2.5 \cdot 10^6$	$n_{\text{total}} = 10^{15}$	$\alpha \approx 0.43 \cdot 10^{12} cm^{-3} s^{-1}$

The distinctive non-uniform distribution of activity on the surface of the investigated *TiD* was observed during both intermediate analyses of the radioluminographic plate after 19 *hours* (control) and after 65 *hours*. This observation validates the stable distribution of fusion regions and beta activity in the same locations, aligning with the microstructure of the target. It has been demonstrated that the mean free path of electrons formed during beta decay of tritium in a flat layer of titanium crystal corresponds to $<l_\beta> \approx 0.4 - 0.5\ \mu m$.

The final parameters of tritium fusion stimulated by a thermal wave are presented in Table 4.

These data correspond to the rate of stimulated nuclear tritium fusion

$$\eta_{H^3} = \begin{cases} T_0 = 40min, & \alpha_{40}/n_{H^2} \approx 2.1 \cdot 10^{-11} \\ T_0 = 20min, & \alpha_{20}/n_{H^2} \approx 0.52 \cdot 10^{-11} \end{cases} \ created\ H^3\ nuclei/sec{\cdot}H^2\ nucleus. \tag{17}$$

A significant nonlinear (quadratic) increase in the total concentration n_{total} of LENR and a linear increase in the rate of these reactions with an extended duration of the temperature wave action indicates an active nonlinear influence of this wave on the conditions for LENR implementation. Such irradiation not only stimulates LENR but also establishes conditions for more efficient LENR, potentially due to the formation of additional nanocracks in the titanium matrix with deuterium or deformation of existing nanocracks (see section 2.1 above).

4. Conclusions

The results obtained demonstrate that undamped temperature waves with frequencies (12), formed during cavitation of a water jet, can propagate over long distances without absorption. These frequencies are determined by the local thermal relaxation time τ in the material medium through which these waves travel.

These waves can effectively stimulate LENR in distant targets. The experiments conducted to stimulate dd-fusion in a distant *TiD* target using such waves reveal that the probability and rate η_{H^3} of tritium fusion in the $d + d = H^3 + p$ reaction are approximately 10^8 times higher than the probability and rate η_{He^4} of He^3 fusion and neutron generation in the alternative $d + d = He^3 + n$ reaction. These findings illustrate a fundamental distinction between LENR and similar reactions involving particles with high real (not virtual) energy. Additional differences between LENR and hot fusion were discussed in [13], [14], [22]–[24].

The reliability of the experimental results obtained is confirmed by several factors. In particular, plastic CR-39 type detectors are stored in the laboratory for a fairly long time, and they remain completely clean. The absence of radioactive background in the laboratory is also confirmed by the result that the concentration of registered active centers on the back side of the *TiD* targets increases approximately proportionally to the duration of irradiation with a thermal wave (20 and 40 *min*). This is clearly seen when comparing Fig. 3a and 3b.

The same effect of direct dependence of the total number of registered particles on the surface of the track detector on the time of irradiation by a thermal wave occurs when studying the reaction with the formation of nuclei He^3. Also convincing confirmation of the reliability of the results is the complete axial symmetry of the orientations of the tracks from He^3 nuclei (Fig. 2a), which is associated with the axial symmetry of both the source of thermal waves and the *TiD* target when recording tracks behind the rear surface of this target.

The results of additional studies of the nuclear fusion under consideration (including the possibility of alpha particle He^4 formation in the process of implementing the third reaction (15)) will be discussed in the future after the completion of additional experiments.

References

[1] V.I.Vysotskii, V.B.Vassilenko, A.O.Vasylenko. Generation and propagation of undamped temperature waves under pulse action on a target surface, *J. Surface Invest*., **8** (2014) 367–373.

[2] V.I.Vysotskii, A.A.Kornilova, A.O.Vasylenko, V.I.Tomak. Detection and investigation of undamped temperature waves excitation under water jet cavitation. *J. Surface Invest.*, **8** (2014) 1186–1192.

[3] V.I. Vysotskii, A.A.Kornilova, A.O.Vasilenko. Observation and investigation of X-Ray and thermal effects at cavitation. *Current Science*, **108** (2015) 114–119.

[4] V.I.Vysotskii, A.A.Kornilova, A.O.Vasylenko, T.B.Krit, M.V.Vysotskyy. On the long-range detection and study of undamped directed temperature waves generated during the interaction between a cavitating water jet and targets. *J. Surface Invest*, **11** (2017) 749–755.

[5] V.I.Vysotskii, A.A.Kornilova, T.Krit, S.Gaydamaka. Generation and detection of undamped temperature waves at large distance in LENR related experiments. *J. Condensed Matter Nucl. Sci.* **29** (2019) 368–375.

[6] A.A.Kornilova, V.I.Vysotskii, T. Krit, M.V.Vysotskyy, S.N.Gaydamaka. Study of the influence of remote undamped temperature waves on nuclear fusion, *J. Surface Invest.*, **14** (2020) No. 1, pp. 117–123.

[7] V.I.Vysotskii, A.A.Kornilova, P.L.Hagelstein, T.B. Krit, S.N.Gaydamaka, M.V.Vysotskyy. Distant behind-screen action of undamped temperature waves (long-distance propagation, X-Ray generation, LENR stimulation), *J. Condensed Matter Nucl. Sci.* 33 (2020), 296–304.

[8] W.M.Preston, Nuclear Reactions Involving Few Nucleons, *Addison–Wesley*, Reading, Massachusetts, 1962.

[9] R.C.Johnson, Alpha Clustering and Nuclear Molecules", *Reports on Progress in Physics*, 1982**,** Vol. **45** (1982) 625–683; DOI: 10.1088/0034-4885/45/6/002

[10] V.I.Vysotskii, M.V.Vysotskyy. Features of correlated states and a mechanism of self-similar selection of nuclear reaction channels involving low-energy charged particles. *J. Exp. Theor. Phys.*, **128**, No. 6 (2019), 856–864.

[11] V.I.Vysotskii, M.V.Vysotskyy, Coherent correlated states and low-energy nuclear reactions in non stationary systems. *European Phys. Jour.* A, **49** (2013), 99.

[12] V.I.Vysotskii, S.V.Adamenko, M.V.Vysotskyy, Acceleration of low energy nuclear reactions by formation of correlated states of interacting particles in dynamical systems. *Annals of Nuclear energy*, **62** (2013), 618.

[13] V.I.Vysotskii, M.V.Vysotskyy. Correlated states and transparency of a barrier for low-energy particles at monotonic deformation of a potential well with dissipation and a stochastic force. *J. Exp. Theor. Phys.,* **118**(4) (2014), 534.

[14] V.I.Vysotskii, M.V.Vysotskyy. Coherent correlated states of interacting particles – the possible key to paradoxes and features of LENR, *Current Science*, **108** (2015), 524.

[15] V.I.Vysotskii, M.V.Vysotskyy. Application of correlated wave packets for stimulation of LENR in remote targets, *J. Condensed Matter Nucl. Sci.*, **33** (2020), 305–313.

[16] V.I.Vysotskii, M.V.Vysotskyy. Features of correlated states and a mechanism of self-similar selection of nuclear reaction channels involving low-energy charged particles, *J. Exp. Theor. Phys.*, **128** (2019), 856–864.

[17] V.I.Vysotskii, M.V.Vysotskyy. Universal mechanism of LENR in physical and biological systems on the base of coherent correlated states of interacting particles. *Cold Fusion. Advances in Condensed Matter Nuclear Science*, Edd. by J.P. Biberian. Elsevier, 2020, CHAPTER 17, 333–370.

[18] E.Schrödinger. Heisenbergschen Unschärfeprinzip. *Ber. Kgl. Akad. Wiss*., S**24** (1930) 296.

[19] H.P.Robertson. A general formulation of the uncertainty principle and its classical interpretation, *Phys.Rev*.A, **35**, (1930), 667.

[20] A.A.Kornilova, V.I.Vysotskii et al. The problem and implementation of sustainable generation of alpha particles by TiD located in a thermal wave field, *Engineering physics,* #5, (2018), 14–22.

[21] Stephanie Cockcroft, Peter E. Dyer, Craig S. Moore, Christopher D. Walton∂ 2009; https://www.researchgate.net/publication/251891483/figure/fig6/AS%3A668690219560964%401536439580273/SEM-images-of-the-tracks-etched-in-CR39-exposed-to-the-alpha-source-and-chemically-etched.ppm

[22] V.I.Vysotskii, M.V.Vysotskyy. Self-controlled flashing nuclear fusion in stationary magnetized low-temperature plasma. *Fusion Sci. and Technology*, 79:5 (2023), 537–552.

[23] V.I.Vysotskii, M.V.Vysotskyy. Manifestations in nature of self-controlled quasi-stationary nuclear fusion into magnetized low-temperature hydrogen plasma. Frontiers Materials, *Sec. Quantum Materials*, vol.11 (2024). https://doi.org/10.3389/fmats.2024.1502051.

[24] V.I.Vysotskii, M.V.Vysotskyy. Current status of the coherent correlated states for explanation of LENR. *J. Condensed Matter Nucl. Sci.* 39 (2025) 165–184.